

A Density Functional Theory Investigation of Fe–N–O Bonding in Heme Proteins and Model Systems

Yong Zhang, William Gossman, and Eric Oldfield*

Contribution from the Department of Chemistry, 600 South Mathews Avenue,
University of Illinois at Urbana-Champaign, Urbana, Illinois 61801

Received June 3, 2003; Revised Manuscript Received August 22, 2003; E-mail: eo@chad.scs.uiuc.edu

Abstract: We report the results of a series of density functional theory (DFT) calculations of the Mössbauer quadrupole splittings and isomer shifts in NO heme model compounds, together with the results of calculations of the Mössbauer quadrupole splittings, isomer shifts, and electron paramagnetic resonance hyperfine coupling constants in a model Fe(II)(NO)(imidazole) complex as a function of Fe–NO bond length and Fe–N–O bond angle. The results of the Mössbauer quadrupole splitting and isomer shift calculations on the NO heme model compounds show good accord between theory and experiment, with the largest errors being observed for structures having the largest crystallographic R_1 values. The results of the property surface calculations were then used to calculate Fe–NO bond length and Fe–N–O bond angle probability surfaces (Z-surfaces) for a nitrosyl hemoglobin, using, in addition, an energy filter. The results obtained yielded a most probable Fe–NO bond length (r) of 1.79 Å and an Fe–N–O bond angle (β) of 136°–137°. This bond length is somewhat longer than those observed in most model compounds but may be due, at least in part, to hydrogen bond formation with the distal His residue. Bond elongation was also observed in a geometry optimized Fe(II)(NO)(imidazole) complex hydrogen bonded to an imidazole residue, in which we find $r = 1.76$ – 1.78 Å and $\beta = 137$ °– 138 °. The computed bond angles are close to the canonical ~ 140 ° value found in most model systems. Highly bent Fe–N–O bond angles or very long Fe–NO bond lengths seem unlikely to occur in proteins, due to their high energies. We also investigated the molecular orbitals and spin densities in each of the six coordinate systems investigated and found the orbitals and spin densities to be generally similar those described previously for five coordinate systems. Taken together, these results show that Mössbauer quadrupole splittings and isomer shifts, in addition to electron paramagnetic resonance hyperfine coupling constants, can now be calculated for nitrosyl heme systems with relatively good accuracy and that the results so obtained can be used to determine Fe–N–O geometries in metalloproteins. The Z-surface approach is thus applicable to both diamagnetic (CO) and paramagnetic (NO) heme proteins with in both cases the metal–ligand binding geometries found in the proteins being very close to those seen in model systems.

Introduction

The topic of how small molecule ligands (O_2 , CO, and NO) bind to heme proteins and heme model systems has been of considerable interest for many years,^{1–4} with particular emphasis being placed on the geometric structures of these small molecule ligands bound to iron. In all cases, a wide range of geometries have been reported in proteins, but this range of geometries has always been found to be much smaller in model systems.^{5–7} On one hand, this could indicate interesting and potentially

important interactions between the small molecule ligand and the protein, but on the other hand, it could simply reflect the difficulty of accurately determining such bond lengths and bond angles in protein molecules, due to the much lower resolution available in proteins versus small molecule (heme model) structures.² In previous work,⁸ we investigated the topic of CO bonding to myoglobin using a combination of Mössbauer and nuclear magnetic resonance spectroscopic techniques, together with quantum chemical calculations, and we found that CO bound in a relatively undistorted or linear geometry to myoglobin, with tilt (τ) and bend (β) angles of ca. 4° and 7°, respectively. These results were considerably different to those

- (1) (a) Pauling, L. *Nature* **1964**, *203*, 182–183. (b) Weiss, J. *Nature* **1964**, *203*, 183.
- (2) Ray, G. B.; Li, Z.-Y.; Ibers, J. A.; Sessler, J. L.; Spiro, T. G. *J. Am. Chem. Soc.* **1994**, *116*, 162–176.
- (3) Lim, M.; Jackson, T. A.; Anfinsen, P. A. *Science* **1995**, *269*, 962–966.
- (4) (a) Ding, X. D.; Weichsel, A.; Andersen, J. F.; Shokhireva, T. K.; Balfour, C.; Pierik, A. J.; Averill, B. A.; Montfort, W. R.; Walker, F. A. *J. Am. Chem. Soc.* **1999**, *121*, 128–138. (b) Maes, E. M.; Walker, F. A.; Montfort, W. R.; Czernuszewicz, R. S. *J. Am. Chem. Soc.* **2001**, *123*, 11664–11672.
- (5) (a) Quillin, M. L.; Arduini, R. M.; Olson, J. S.; Phillips, G. N., Jr. *J. Mol. Biol.* **1993**, *234*, 140–155. (b) Kuriyan, J.; Wilz, S.; Karplus, M.; Petsko, G. A. *J. Mol. Biol.* **1986**, *192*, 133–154. (c) Salzmänn, R.; Ziegler, C. J.; Godbout, N.; McMahon, M. T.; Suslick, K. S.; Oldfield, E. *J. Am. Chem. Soc.* **1998**, *120*, 11323–11334.

- (6) (a) Shaanan, B. *J. Mol. Biol.* **1983**, *171*, 31–59. Steigemann, W.; Weber, E. In *Hemoglobin and Oxygen Binding*; Ho, C., Ed.; Elsevier Biomedical: New York, 1982; pp 19–24. (b) Phillips, S. E. V. *J. Mol. Biol.* **1980**, *142*, 531–554. (c) Godbout, N.; Sanders, L. K.; Salzmänn, R.; Havlin, R. H.; Wojdelski, M.; Oldfield, E. *J. Am. Chem. Soc.* **1999**, *121*, 3829–3844.
- (7) (a) Wylie, G. R. A.; Scheidt, W. R. *Chem. Rev.* **2002**, *102*, 1067–1089. (b) Scheidt, W. R.; Ellison, M. K. *Acc. Chem. Res.* **1999**, *32*, 350–359.
- (8) McMahon, M.; deDios, A. C.; Godbout, N.; Salzmänn, R.; Laws, D. D.; Le, H.; Havlin, R. H.; Oldfield, E. *J. Am. Chem. Soc.* **1998**, *120*, 4784–4797.

obtained in earlier crystallographic (and other) investigations, but were later verified by a new high-resolution crystallographic structure obtained by using synchrotron radiation,⁹ and are of interest in the context of the question of CO/O₂ discrimination by proteins. In the case of NO binding to heme proteins, there are again a very wide range of geometries reported for proteins in the literature^{10–13} but a much smaller range for NO bound to heme (or more specifically Fe(II)-porphyrin) model systems,^{7,14–20} where structures can reasonably be expected to be known with high accuracy and precision. For example, Fe–N–O bond angles varying between 110 and 155° have been reported in metalloproteins, but in metalloporphyrin model systems, the range is only between 137.4° and 143.7°.⁷ Likewise, Fe–NO bond lengths have been reported to vary between 1.72 and 2.0 Å in metalloproteins but only between 1.72 and 1.84 Å in model systems.⁷ In this work, we have therefore begun to use a combination of experimental (Mössbauer quadrupole splittings and isomer shifts, together with electron paramagnetic resonance hyperfine couplings) and quantum chemical techniques to try to probe in more detail metal–ligand geometries in the paramagnetic NO heme proteins nitrosylhemoglobin and nitrosylmyoglobin, since the topic of NO binding to heme Fe(II) is of considerable current interest in the context of NO transport and the regulation of vascular tension.²¹ The bond angle results obtained for HbNO and MbNO are found to be very close to the canonical values found in model compounds, while the Fe–NO bond distances are somewhat elongated, due we propose to an electrostatic (hydrogen bond) interaction between NO and the distal His residue. Highly bent geometries appear to be unlikely, based on their calculated energies.

Computational Aspects

The ⁵⁷Fe quadrupole splitting arises from the nonspherical nuclear charge distribution in the $I^* = 3/2$ excited state in the presence of an electric field gradient at the ⁵⁷Fe nucleus, while the isomer shift arises from differences in the electron density at the nucleus between the absorber (the molecule or system of interest) and a reference compound (usually α -Fe at 300 K). The former effect is related to the components of the electric field gradient tensor at the nucleus as follows:²²

$$\Delta E_Q = \frac{1}{2}eQV_{zz}\left(1 + \frac{\eta^2}{3}\right)^{1/2} \quad (1)$$

where e is the electron charge, Q is the quadrupole moment of the $E^* = 14.4$ keV excited state, and the principal components of the EFG tensor are labeled according to the convention

- (9) Kachalova, G. S.; Popov, A. N.; Bartunik, H. D. *Science* **1999**, *284*, 475–476.
 (10) Deatherage, J. F.; Moffat, K. *J. Mol. Biol.* **1979**, *134*, 401–417.
 (11) Brucker, E. A.; Olson, J. S.; Ikeda-Saito, M.; Phillips, G. N. *Proteins: Struct., Funct., Genet.* **1998**, *30*, 352–356.
 (12) Harutyunyan, E. H.; Safonova, T. N.; Kuranova, I. P.; Popov, A. N.; Teplyakov, A. V.; Obmolova, G. V.; Valnshtein, B. K.; Dodson, G. G.; Wilson, J. C. *J. Mol. Biol.* **1996**, *264*, 152–161.
 (13) Edwards, S. L.; Poulos, T. L. *J. Biol. Chem.* **1990**, *265*, 2588–2595.
 (14) Scheidt, W. R.; Piccolo, P. L. *J. Am. Chem. Soc.* **1976**, *98*, 1913–1919.
 (15) Ellison, M. K.; Scheidt, W. R. *J. Am. Chem. Soc.* **1997**, *119*, 7404–7405.
 (16) Scheidt, W. R.; Frisse, M. E. *J. Am. Chem. Soc.* **1975**, *97*, 17–21.
 (17) Ellison, M. K.; Schulz, C. E.; Scheidt, W. R. *J. Am. Chem. Soc.* **2002**, *124*, 13833–13841.
 (18) Ellison, M. K.; Scheidt, W. R. *J. Am. Chem. Soc.* **1999**, *121*, 5210–5219.
 (19) Ellison, M. K.; Schulz, C. E.; Scheidt, W. R. *Inorg. Chem.* **1999**, *38*, 100–108.
 (20) Ellison, M. K.; Schulz, C. E.; Scheidt, W. R. *Inorg. Chem.* **2000**, *39*, 5102–5110.
 (21) Luchsinger, B. P.; Rich, E. C.; Gow, A. J.; Williams, E. M.; Stamler, J. S.; Singel, D. J. *Proc. Natl. Acad. Sci. U.S.A.* **2003**, *100*, 461–466.
 (22) Debrunner, P. G. In *Iron Porphyrins*; Lever, A. B. P., Gray, H. B., Eds.; VCH Publishers: New York, 1989; Vol. 3, pp 139–234.

$$|V_{zz}| > |V_{yy}| > |V_{xx}| \quad (2)$$

with the asymmetry parameter being given by

$$\eta = \frac{V_{xx} - V_{yy}}{V_{zz}} \quad (3)$$

The isomer shift in ⁵⁷Fe Mössbauer spectroscopy is given by²²

$$\delta_{\text{Fe}} = E_A - E_{\text{Fe}} = \frac{2\pi}{3}Ze^2(\langle R^2 \rangle^* - \langle R^2 \rangle)(|\psi(0)|_A^2 - |\psi(0)|_{\text{Fe}}^2) \quad (4)$$

where Z represents the atomic number of the nucleus of interest (iron) and R, R^* are average nuclear radii of the ground and excited states of ⁵⁷Fe. Since $|\psi(0)|_{\text{Fe}}^2$ is a constant, the isomer shift (from Fe) can be written as

$$\delta_{\text{Fe}} = \alpha[\rho(0) - c] \quad (5)$$

where α is the so-called calibration constant and $\rho(0)$ is the computed charge density at the iron nucleus. Both α and c can be obtained from the correlation between experimental δ_{Fe} values and the corresponding computed $\rho(0)$ data in a training set. Then, one can use eq 5 to predict δ_{Fe} for a new molecule from its computed $\rho(0)$, basically as described in detail elsewhere for a wide variety of heme and other model systems.²³

The hyperfine interaction tensor \tilde{A} is a second rank tensor, which can be separated into isotropic/Fermi-contact (A_{iso}) and anisotropic/dipolar (\tilde{T}) components:

$$\tilde{A} = A_{\text{iso}}\tilde{I} + \tilde{T} = \left[\frac{1}{3}\text{Tr}(\tilde{A})\right]\tilde{I} + \tilde{T} \quad (6)$$

where \tilde{I} is a unit matrix. The isotropic hyperfine coupling constant (A_{iso}) of a given nucleus can be computed from the spin density at that nucleus ($\rho_{\alpha\beta}$), using the relation:²⁴

$$A_{\text{iso}} = \frac{8\pi}{3}\hbar\gamma_n g_e \beta_e \rho_{\alpha\beta} \quad (7)$$

where \hbar is Planck's constant divided by 2π , γ_n is the nuclear gyromagnetic ratio, g_e is the free electron g -factor, and β_e is the Bohr magneton. The dipolar term (\tilde{T} -tensor) is traceless and its elements are given by²⁴

$$T_{ij} = -\hbar\gamma_n g_e \beta_e \left\langle \frac{r^2 \delta_{ij} - 3r_i r_j}{r^5} \right\rangle \quad (8)$$

where r is the distance between the atom containing the unpaired electron and the nucleus with nonzero spin and r_i is the i -th space coordinate. Therefore, each principal component of the hyperfine interaction tensor ($A_{ii}, i = 1, 2, 3$) is evaluated as the sum of A_{iso} and T_{ii} .

To calculate ΔE_Q , we used the Gaussian 98 program²⁵ to evaluate the principal components of the electric field gradient tensor at the

- (23) Zhang, Y.; Mao, J.; Oldfield, E. *J. Am. Chem. Soc.* **2002**, *124*, 7829–7839.
 (24) Drago, R. S. *Physical Methods in Chemistry*; W. B. Saunders Company: Philadelphia, PA, 1977.
 (25) Frisch, M. J.; Trucks, G. W.; Schlegel, H. B.; Scuseria, G. E.; Robb, M. A.; Cheeseman, J. R.; Zakrzewski, V. G.; Montgomery, J. A., Jr.; Stratmann, R. E.; Burant, J. C.; Dapprich, S.; Millam, J. M.; Daniels, A. D.; Kudin, K. N.; Strain, M. C.; Farkas, O.; Tomasi, J.; Barone, V.; Cossi, M.; Cammi, R.; Mennucci, B.; Pomelli, C.; Adamo, C.; Clifford, S.; Ochterski, J.; Petersson, G. A.; Ayala, P. Y.; Cui, Q.; Morokuma, K.; Malick, D. K.; Rabuck, A. D.; Raghavachari, K.; Foresman, J. B.; Cioslowski, J.; Ortiz, J. V.; Baboul, A. G.; Stefanov, B. B.; Liu, G.; Liashenko, A.; Piskorz, P.; Komaromi, I.; Gomperts, R.; Martin, R. L.; Fox, D. J.; Keith, T.; Al-Laham, M. A.; Peng, C. Y.; Nanayakkara, A.; Challacombe, M.; Gill, P. M. W.; Johnson, B.; Chen, W.; Wong, M. W.; Andres, J. L.; Gonzalez, C.; Head-Gordon, M.; Replogle, E. S.; Pople, J. A. *Gaussian 98*; Gaussian, Inc.: Pittsburgh, PA, 1998.

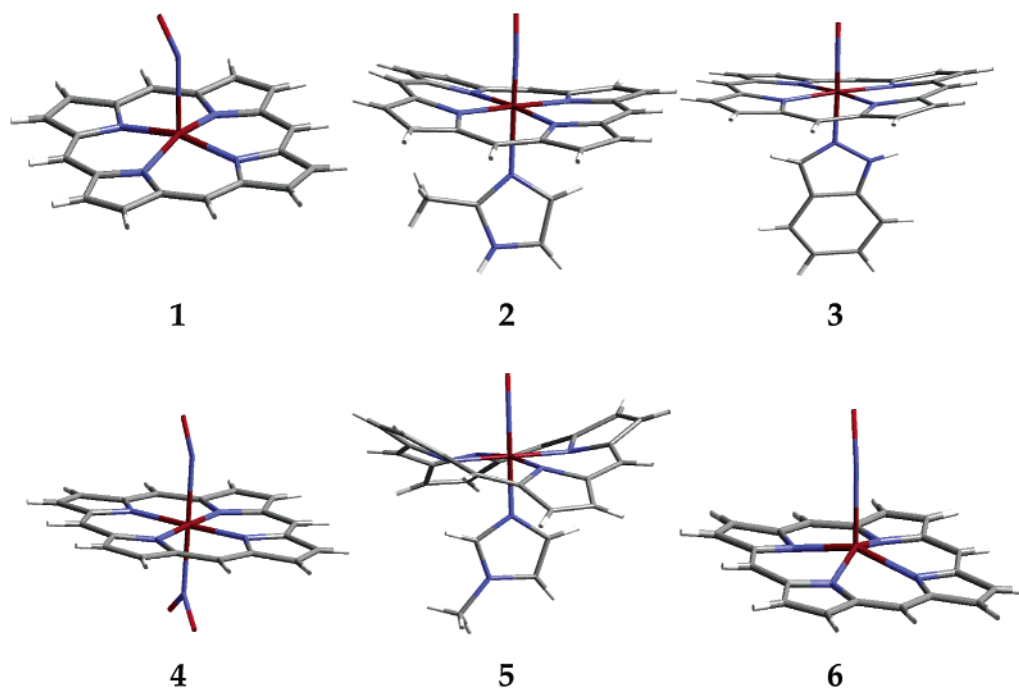


Figure 1. Structures of nitrosylheme model complexes (1–6) used in the calculations (Fe—dark red; N—blue; O—red; C—dark gray; H—light gray).

^{57}Fe nucleus (V_{ii}), and then we used eq 1 to deduce ΔE_Q , using a precise recent determination of $Q = 0.16(\pm 5\%) \times 10^{-28} \text{ m}^2$,²⁶ a value previously found to permit excellent accord between theory and experiment in a broad range of systems.^{27,28} We used the same computational approach as in our previous studies, which enabled accurate predictions of Mössbauer quadrupole splittings²⁷ and isomer shifts²³ as well as NMR hyperfine shifts²⁹ in iron complexes containing d^2 to d^8 iron and in all spin states ($S = 0, 1/2, 1, 3/2, 2, 5/2$): a Wachter's basis (621111111/33111111/3111) for Fe,³⁰ 6-311G* for all the other heavy atoms, and 6-31G* for hydrogens. We investigated use of both the pure density functional BPW91 (the Becke 88 exchange³¹ and PW91 correlation functionals³²) and the hybrid functional B3LYP (Becke's three-parameter functional³³ with the LYP correlation functional³⁴), which includes the effects of Hartree–Fock exchange.

To calculate δ_{Fe} values, we read the wave functions from the Gaussian 98 calculations into the AIM 2000 program,³⁵ in order to evaluate the charge density at the iron nucleus, $\rho(0)$. Then, we evaluated the isomer shifts by using the two equations derived previously:²³

$$\delta_{\text{Fe}} = -0.471[\rho(0) - 11617.30] \quad (\text{BPW91}) \quad (9)$$

$$\delta_{\text{Fe}} = -0.404[\rho(0) - 11614.16] \quad (\text{B3LYP}) \quad (10)$$

Spin unrestricted and spin restricted methods were used for the paramagnetic and diamagnetic systems, respectively. For the A_{ii} calculations, the A_{iso} and T_{ii} hyperfine (dipolar interaction) values are taken directly from the output of the Gaussian 98 program.

Unlike the situation with Fe–CO systems, there are no Mössbauer results on six-coordinate $S = 1/2$ NO hemes containing an axial imidazole base. Consequently, we investigated the six systems (1–6) shown in Figure 1 which have either $S = 1/2$ in a five-coordinate geometry or $S = 0$ in both five- and six-coordinate geometries. Complex 1 is the neutral $S = 1/2$ molecule Fe(TPP)(NO) (TPP = *meso*-tetraphenylporphyrinate),^{16,36} while compounds 2–5 are all ferric, six-coordinate NO complexes: 2, [Fe(OEP)(2-MeIm)(NO)]⁺ (OEP = octaethylporphyrinate; 2-MeIm = 2-methylimidazole);¹⁷ 3, [Fe(OEP)(Iz)(NO)]⁺ (Iz = indazole);^{18,20} 4, [Fe(TpivPP)(NO₂)(NO)], (TpivPP = (α, α, α)-tetrakis(*o*-pivalamidophenyl)porphyrin);¹⁹ and 5, [Fe(OEP)(1-MeIm)(NO)]⁺ (1-MeIm = 1-methylimidazole).^{18,37} Compound 6 is the five-coordinate ferric system, [Fe(OEP)(NO)]⁺.²⁰ In this work, as in that described previously,²⁷ side chains on the porphyrin framework were replaced with hydrogen atoms so that only the porphyrin core was retained, as illustrated in Figure 1. Counterions were not included in the property calculations since their effects have previously been shown to be negligible.³⁸

We also carried out a series of energy and property (Mössbauer quadrupole splitting, Mössbauer isomer shift and EPR hyperfine coupling constant) calculations for nine Fe(II)(NO)(imidazole) structures containing different Fe–NO bond lengths (r) and Fe–N–O bond angles (β), the structure parameters which vary widely in protein crystal structures. The bond lengths used were $r = 1.74, 1.86, \text{ and } 1.98 \text{ \AA}$ and the bond angles were $\beta = 111^\circ, 128^\circ, \text{ and } 145^\circ$. This enabled us to construct a series of property surfaces and hence probability or Z-surfaces (as described below) covering most of the structure space which has been proposed to be populated in NO heme proteins.

Results and Discussion

We show in Table 1 the results of our density functional theory Mössbauer quadrupole splitting and isomer shift property calculations for the six iron nitrosylmetalloporphyrins whose structures (1–6) are shown in Figure 1, together with, for

- (26) Dufek, P.; Blaha, P.; Schwarz, K. *Phys. Rev. Lett.* **1995**, *75*, 3545–3548.
 (27) Zhang, Y.; Mao, J.; Godbout, N.; Oldfield, E. *J. Am. Chem. Soc.* **2002**, *124*, 13921–13930.
 (28) Godbout, N.; Havlin, R.; Salzmann, R.; Debrunner, P. G.; Oldfield, E. *J. Phys. Chem. A* **1998**, *102*, 2342–2350.
 (29) Mao, J.; Zhang, Y.; Oldfield, E. *J. Am. Chem. Soc.* **2002**, *124*, 13911–13920.
 (30) Wachters, A. J. H. *J. Chem. Phys.* **1970**, *52*, 1033–1036. Wachters, A. J. H. *IBM Technology Report RJ584*; 1969.
 (31) Becke, A. D. *Phys. Rev. A* **1988**, *38*, 3098–3100.
 (32) Perdew, J. P.; Burke, K.; Wang, Y. *Phys. Rev. B* **1996**, *54*, 16533–16539.
 (33) Becke, A. D. *J. Chem. Phys.* **1993**, *98*, 5648–52.
 (34) Lee, C.; Yang, W.; Parr, R. G. *Phys. Rev. B* **1988**, *37*, 785–789.
 (35) (a) Biegler-König F. *AIM2000*, version 1.0; University of Applied Science: Bielefeld, Germany. (b) Bader, R. F. W. *Atoms in Molecules: A Quantum Theory*; Oxford University Press: Oxford, 1990.

- (36) Nasri, H.; Ellison, M. K.; Chen, S.; Huynh, B. H.; Scheidt, W. R. *J. Am. Chem. Soc.* **1997**, *119*, 6274–6283.
 (37) Schünemann, V.; Benda, R.; Trautwein, A. X.; Walker, F. A. *Isr. J. Chem.* **2000**, *40*, 9–14.
 (38) Zhang, Y.; Oldfield, E. *J. Phys. Chem. B* **2003**, *107*, 7180–7188.

Table 1. DFT Calculations on NO Heme Model Compounds

compound	R_1^a (%)	S	method ^b	T (K)	ΔE_Q (mm s ⁻¹)	δ_{Fe} (mm s ⁻¹)	$\rho_{\alpha\beta}^{Fe\ c}$ (e)	$\rho_{\alpha\beta}^{NO\ c}$ (e)
1 Fe(TPP)(NO)	4.4 [16]	1/2	expt [36]	4.2	1.24	0.35	0.89	0.10
			BPW91		1.27	0.39		
			B3LYP		1.14	0.36		
2 [Fe(OEP)(2-MeIm)(NO)] ⁺	8.66 [17]	0	expt [17]	4.2	1.88	0.05	1.00	0.04
			BPW91		1.93	0.08		
			B3LYP		1.93	0.06		
3 [Fe(OEP)(Iz)(NO)] ⁺	9.12 [18]	0	expt [20]	4.2	1.99	0.02	1.00	0.04
			BPW91		1.91	0.08		
			B3LYP		1.91	0.01		
4 [Fe(TpivPP)(NO ₂)(NO)]	5.82 [19]	0	expt [19]	4.2	1.43	0.09	1.00	0.04
			BPW91		1.06	0.14		
			B3LYP		1.18	0.09		
5 [Fe(OEP)(1-MeIm)(NO)] ⁺	6.14 [18]	0	expt [37]	4.2	1.64	0.02	1.00	0.04
			BPW91		1.10	0.01		
			B3LYP		1.91	0.06		
6 [Fe(OEP)(NO)] ⁺	11.11 [20]	0	expt [20]	4.2	1.64	0.20	1.00	0.04
			BPW91		2.27	0.23		
			B3LYP		2.36	0.17		
7 Fe(OEP)(NO) ^d	4.12 [15]	1/2	expt [39]	100	1.26	0.35	0.94	0.06
			BPW91		1.32	0.41		
			B3LYP		1.21	0.36		
8 Fe(OEP)(NO) ^d	4.21 [15]	1/2	expt [39]	100	1.26	0.35	0.88	0.10
			BPW91		1.33	0.39		
			B3LYP		1.24	0.35		

^a Structural references are given in brackets. ^b Experimental references are given in brackets. ^c $\rho_{\alpha\beta}^{Fe}$ and $\rho_{\alpha\beta}^{NO}$ are the Mulliken spin densities of iron and the nitrosyl moiety, respectively. ^d Previous work from refs 23 and 27 for two different structures.

completeness, the results for the two five-coordinate $S = 1/2$ systems (**7**, **8**: the two molecules in the unit cell of Fe(II)-(OEP)(NO)^{15,39}) reported previously.^{23,27} Also, we show the computed spin densities on Fe, for **1**, **7**, and **8**. Both BPW91 and B3LYP results are shown in the table, and a graphical comparison of the experimental quadrupole splittings and isomer shifts with the computed values is shown in Figure 2. The results for all eight nitrosylmetalloporphyrins are shown as solid circles (●) while the results for the other metalloporphyrins investigated previously^{23,27} (covering all common spin and oxidation states) are shown as open circles (○). The results for the nitrosylmetalloporphyrins cover a relatively small range in property values but, nevertheless, lie on the correlation line established previously.^{23,27} For example, for ΔE_Q , when using the BPW91 functional, we previously found $R^2 = 0.975$ for the theory versus experiment correlation for $N = 23$ compounds with a slope of 0.99 and an rmsd of 0.30 mm s⁻¹. With the $N = 29$ compound data set containing the six new nitrosylmetalloporphyrins, we now find $R^2 = 0.970$, a slope of 0.99, and an rmsd of 0.32 mm s⁻¹. There is, however, a marked scatter in the computed results when considering solely the nitrosyl compound (**1–8**) ΔE_Q results, although this effect is not seen in the δ_{Fe} calculations (Figure 2C,D). This is consistent with our general observation that accurate ΔE_Q results are rather more difficult to calculate than are Mössbauer δ_{Fe} values, and previously we attributed this to the larger structure sensitivity of the electric field gradient tensor (V_{ii}) calculation, as opposed to the charge density $\rho(0)$ calculations. While this might at first sight appear surprising, since it is the δ_{Fe} calculations which lack corrections for second-order Doppler effects, as may be seen in Figure 3, there is clearly a general correlation between the errors in the computed ΔE_Q values and the quality of the crystal structure used (as determined by conventional crystallographic R_1 values). That

is, the largest errors come from the largest R_1 value structures. In two cases (**2** and **3**), there are fortuitously good ΔE_Q property predictions from the lower resolution structures, but more importantly, there are no counterexamples of poor property predictions for high resolution structures. While this point may not appear important, it is in fact important from the standpoint of structure predictions based on property surfaces, as discussed below. That is, the results of Figure 3 imply that much of the error in the ΔE_Q property predictions can be attributed to structural uncertainties rather than major deficiencies in the calculations. This implies, therefore, that it should be possible to use both ΔE_Q and δ_{Fe} Mössbauer properties for structure determination in Fe–NO heme proteins, basically as described before for Fe–CO heme proteins, using the Bayesian or Z-surface approach.⁸

We show in Table 2 the results of Mössbauer quadrupole splitting and isomer shift calculations for a series of Fe(II)-(NO)(imidazole) structures in which the Fe–NO bond lengths and Fe–N–O bond angles were systematically changed: from 1.74 to 1.86 to 1.98 Å and from 111° to 128° to 145°. In addition, we also evaluated the EPR hyperfine coupling components, A_{ii} , at each of the nine geometries, together with the energies of the individual structures (reported in Table 2 with respect to the lowest energy structure found at $r = 1.74$ Å and $\beta = 145^\circ$, in good agreement with the previous result reported by Parrinello and co-workers: $r = 1.72$ Å and $\beta = 138^\circ$ ⁴⁰). For each of these nine structures, the basic structure was taken from the X-ray crystallographic result for Fe(TPP)-(1-MeIm)(NO)¹⁴ and was subject to geometry optimization in which the Fe–N–O tilt angle, the N–O bond length, and the N_p –Fe–N–O torsions were all allowed to relax. The resulting values (BPW91 functional) are all given in Table 2.

(39) Bohle, D. S.; Debrunner, P.; Fitzgerald, J. P.; Hansert, B.; Hung, C.-H.; Thomson, A. J. *Chem. Commun.* **1997**, 91–92.

(40) Rovira, C.; Kunc, K.; Hutter, J.; Ballone, P.; Parrinello, M. *J. Phys. Chem. A* **1997**, *101*, 8914–8925.

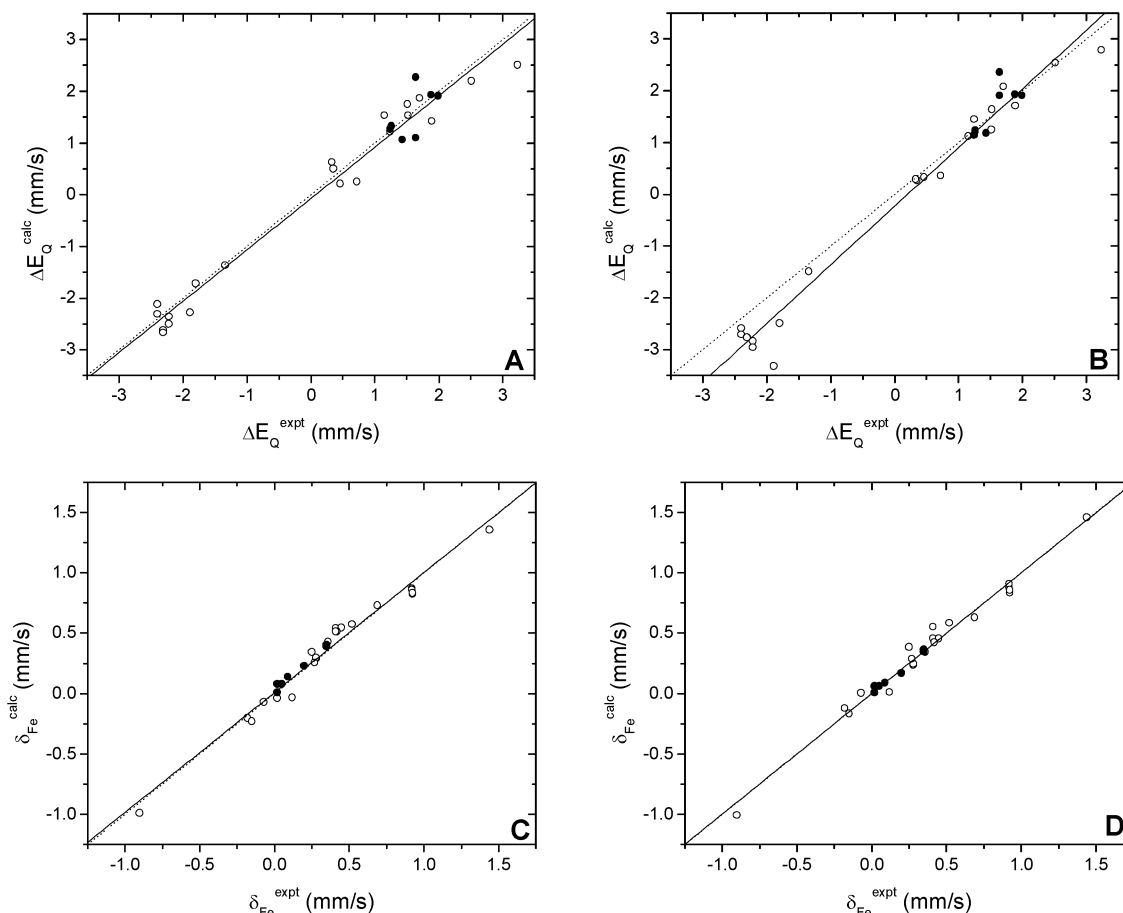


Figure 2. DFT computational results plotted versus the experimental results for NO complexes and other heme model complexes (from refs 23 and 27): (A) ΔE_Q /BPW91; (B) ΔE_Q /B3LYP; (C) δ_{Fe} /BPW91; (D) δ_{Fe} /B3LYP. The NO complexes are represented by the solid circles (●); other structures are represented by open circles (○). The solid lines are the best-fit lines through all the data points. The dotted line is the ideal 45° line with a slope of 1.00 and an intercept of 0.00 mm s^{-1} .

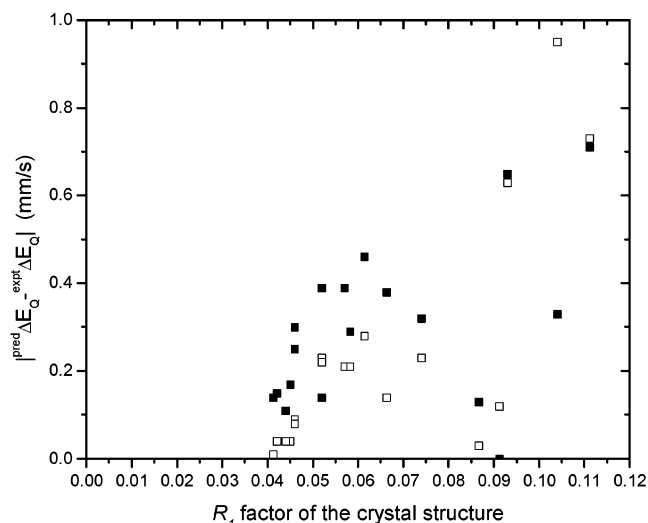


Figure 3. Graph showing differences between predicted (from theory-versus-experiment correlations) and experimental quadrupole splittings as a function of the crystallographic R_1 factors for the heme model systems investigated here and in previous work²⁷ using BPW91 (solid square, ■) and B3LYP (open square, □) functionals.

For the EPR hyperfine coupling constant parameter, we felt it necessary to validate the surface calculations by investigating a model system in which the hyperfine coupling tensor had previously been determined with some precision. We therefore

computed A_{ii} values for the Fe(OEP)(NO) system, which has been investigated experimentally by using single-crystal EPR and where A_{ii} values of 42.5, 44.1, and 55.8 MHz have been reported.⁴¹ We obtained A_{ii} values of (+)43.3, (+)51.2, (+)62.8 and (+)47.0, (+)52.5, (+)65.5 MHz for the two molecules in the unit cell using the BPW91 functional, with $R^2 = 0.928$ and an rms error on the three principal A_{ii} components of 2.63 MHz (for the six tensor components, obtained from the crystallographic structures reported). Results with the B3LYP functional were 25.0, 43.3, 56.4 and 24.6, 44.1, 60.4 MHz for A_{ii} , corresponding to an rms error of 7.48 MHz. The hybrid functional B3LYP clearly performed less well than the pure functional, BPW91, so, consequently, we focused on BPW91 property surfaces (Table 2) since with B3LYP there is a 3-fold larger rms error on the three tensor components than with BPW91.

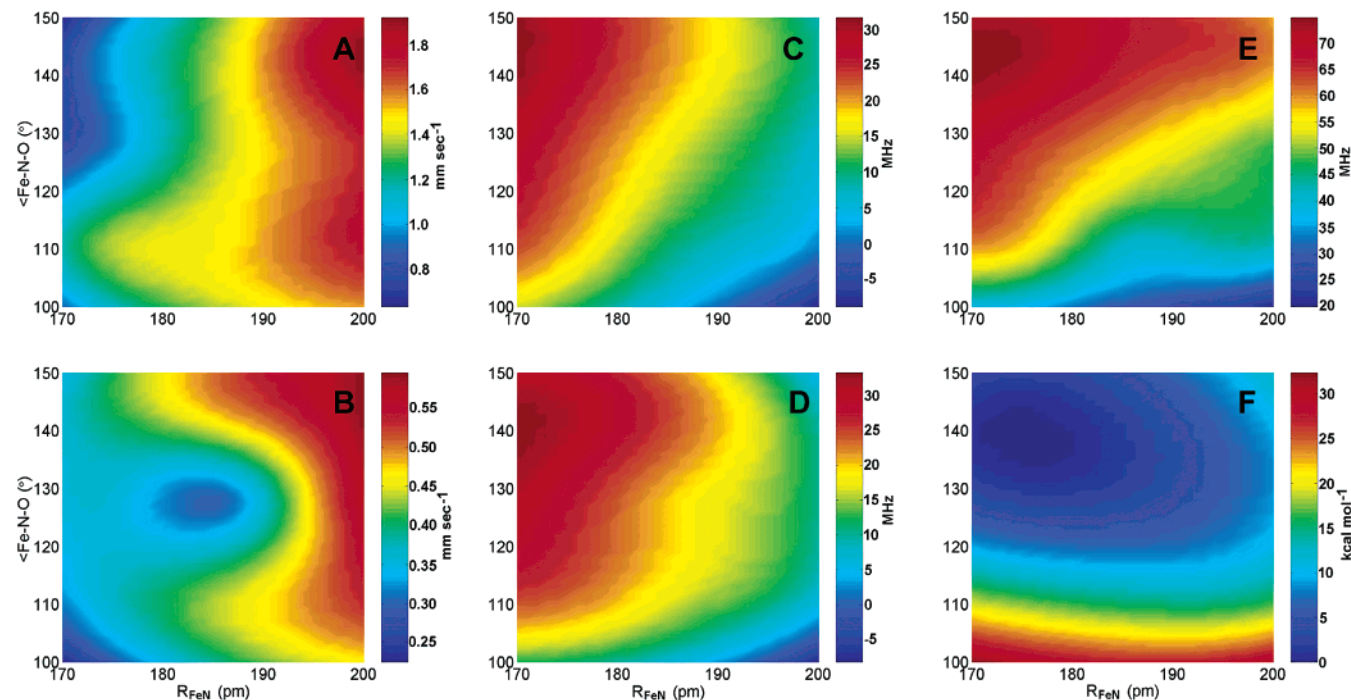
We show in Figure 4 the property surface results obtained from the computational results shown in Table 2. Figure 4A shows the computed quadrupole splittings as a function of Fe–NO bond length (r) and Fe–N–O bond angle (β); Figure 4B shows the isomer shift results, δ_{Fe} (r, β); Figure 4C–E show the hyperfine coupling results, A_{ii} (r, β) (A_{11} – A_{33} , Figure 4C–E, respectively); and Figure 4F is the energy surface, $E(r, \beta)$. In Figure 5, we show the probability or Z-surface results. The

(41) Hayes, P. G.; Ellison, M. K.; Scheidt, W. R. *Inorg. Chem.* **2000**, *39*, 3665–3668.

Table 2. BPW91 Calculated Properties for Optimized Fe(TPP)(1-Melm)(NO) Structures Determined by Varying the Fe–NO Distance (r) and the Fe–N–O Angle (β)

property	$r = 1.74 \text{ \AA}$ $\beta = 111^\circ$	$r = 1.74 \text{ \AA}$ $\beta = 128^\circ$	$r = 1.74 \text{ \AA}$ $\beta = 145^\circ$	$r = 1.86 \text{ \AA}$ $\beta = 111^\circ$	$r = 1.86 \text{ \AA}$ $\beta = 128^\circ$	$r = 1.86 \text{ \AA}$ $\beta = 145^\circ$	$r = 1.98 \text{ \AA}$ $\beta = 111^\circ$	$r = 1.98 \text{ \AA}$ $\beta = 128^\circ$	$r = 1.98 \text{ \AA}$ $\beta = 145^\circ$
R_{NO} (Å)	1.204	1.189	1.182	1.191	1.178	1.174	1.185	1.176	1.165
tilt (deg)	0.5	−0.7	1.0	−0.1	−2.2	0.04	−0.9	−0.7	2.1
NO–NN ^a (deg)	18.7	15.9	9.6	16.9	12.3	9.2	17.7	14.7	11.8
ΔE_{Q} (mm s ^{−1})	1.34	0.91	0.96	1.46	1.38	1.38	1.72	1.67	1.87
δ_{Fe} (mm s ^{−1})	0.36	0.36	0.40	0.44	0.30	0.50	0.52	0.54	0.58
A_{11} (MHz)	20.62	24.88	28.98	9.63	15.62	19.94	3.15	7.71	10.76
A_{22} (MHz)	23.72	28.32	31.49	16.51	19.25	23.94	8.69	12.29	10.90
A_{33} (MHz)	58.23	65.72	73.93	40.91	57.11	66.31	43.75	49.03	62.37
E^b (kcal mol ^{−1})	17.01	2.57	0.69	14.50	3.20	3.20	15.12	7.59	9.48

^a This is the dihedral angle between NO and the closest porphyrin nitrogen. ^b E is the electronic energy referenced to a structure with $r = 1.75 \text{ \AA}$ and $\beta = 139^\circ$ ($E = 0$).

**Figure 4.** Property surfaces for the Fe(P)(1-MeIm)(NO) model: (A) ΔE_{Q} ; (B) δ_{Fe} ; (C) A_{11} ; (D) A_{22} ; (E) A_{33} ; (F) E . Colors reflect the properties.

Z-surface idea has been described several times previously^{8,42–43} and basically involves calculating the conditional or Bayesian probability that a particular set of parameters, such as the bond lengths (r) and bond angles (β) described here, or tilt and bend angles in the case of Fe–C–O bonding in a metalloprotein,⁸ or peptide backbone ϕ and ψ angles in all proteins, enables the reproduction of an experimentally observed property, such as an NMR chemical shift or a Mössbauer isomer shift. That is, the probability Z is defined as

$$Z = \exp\left[-\left(\frac{P_{\text{expt}} - P_{\text{calc}}(r, \beta)}{W}\right)^2\right] \quad (11)$$

where P_{expt} is the experimentally observed value of the property, $P_{\text{calc}}(r, \beta)$ is the calculated value of the property for the given r, β structure coordinate, and W is a search width parameter. A multiple (n -fold) Z-surface can then be readily constructed

simply by multiplying each individual probability or Z-surface and then (optionally) taking the n -th root:

$${}^n Z = \sqrt[n]{\prod Z} \quad (12)$$

We next constructed the experimental property ¹Z-surfaces shown in Figure 5A–J for hemoglobin by using the experimentally observed values of the quadrupole splitting (1.5 mm s^{−1} at both 4.2 K and 100 K),^{44,45} the isomer shift (0.42 and 0.32 mm sec^{−1} at 4.2 K and 100 K, respectively),⁴⁴ and the hyperfine coupling A_{ii} values (29.6, 32.9, 63.6 MHz for the α subunit and 26.9, 44.2, 62.3 MHz for the β subunit, at 85 K).⁴⁶ The W parameters were chosen to yield Z values in the ~ 0.1 – 0.9 range over the entire Z-surfaces in each case, so as to not overemphasize the contributions of any given property to the final result, since the actual experimental (and computational) errors are not always known with high accuracy. However, one

(42) Le, H.; Pearson, J. G.; deDios, A. C.; Oldfield, E. *J. Am. Chem. Soc.* **1995**, *117*, 3800–3807.

(43) Heller, J.; Laws, D. D.; Tomaselli, M.; King, D. S.; Wemmer, D. E.; Pines, A.; Halvin, R. H.; Oldfield, E. *J. Am. Chem. Soc.* **1997**, *119*, 7827–7831.

(44) Pfannes, H.-D.; Bemski, G.; Wajnberg, E.; Rocha, H.; Bill, E.; Winkler, H.; Trautwein, A. X. *Hyperfine Interact.* **1994**, *91*, 797–802.

(45) Oosterhuis, W. T.; Lang, G. *J. Chem. Phys.* **1969**, *50*, 4381–4387.

(46) Utterback, S. G.; Doetschman, D. C.; Szumowski, J.; Rizo, A. K. *J. Chem. Phys.* **1983**, *78*, 5874–5880.

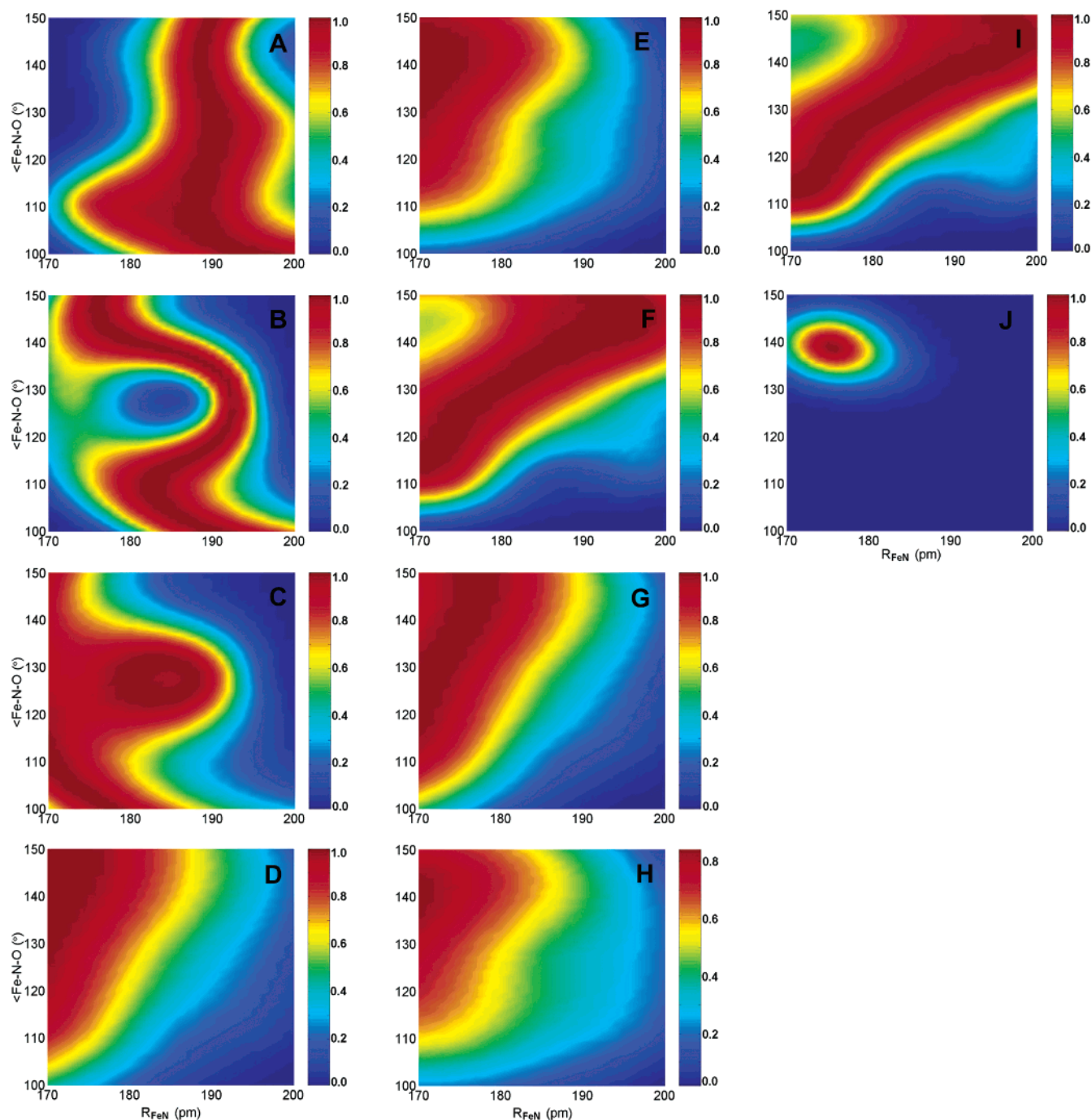


Figure 5. 1Z -surface for HbNO: (A) ΔE_Q 1Z -surface; (B) δ_{Fe} 1Z -surface (4.2 K); (C) δ_{Fe} 1Z -surface (100 K); (D) A_{11} 1Z -surface (α -subunit); (E) A_{22} 1Z -surface (α -subunit); (F) A_{33} 1Z -surface (α -subunit); (G) A_{11} 1Z -surface (β -subunit); (H) A_{22} 1Z -surface (β -subunit); (I) A_{33} 1Z -surface (β -subunit); (J) E 1Z -surface (100 K). Colors reflect the probabilities or Z values as described in the text. The W parameters used for ΔE_Q and δ_{Fe} were 0.30 and 0.077 (0.13 for 100 K surfaces), respectively, while the W parameters used for A_{11} , A_{22} , and A_{33} were 16.47, 15.86, 14.65 and 14.19, 26.30, 13.95 for α - and β -subunits, respectively.

of the ideas behind the use of the conditional probability approach is that the errors from a given property or 1Z -surface prediction tend to average out as the results of more and more Z-surfaces are combined, an idea which has been verified in our previous study of Fe–CO bonding in heme proteins.⁸ In addition, we evaluated the energy “Z-surfaces”, Figure 5J, taken simply to be $\exp(-\Delta E/RT)$ at $T = 100$ K (a temperature close to that of both the EPR (85 K) and the Mössbauer (100 K) data set).

We next investigated the effects of combining multiple 1Z surfaces, eq 12, to determine r and β , as shown in Figure 6. Figure 6A shows the 2Z (r, β) surface obtained by using ΔE_Q and δ_{Fe} data obtained for HbNO at 4.2 K, and Figure 6B, the results obtained by using data obtained at 100 K. For the 2Z 4.2 K surface, there is a broad range of high probability centered at ~ 1.85 Å, covering a large range in β , but this is more centered at 100 K, Figure 6B. 3Z -surfaces for the α and β chain A_{ii} values are shown in Figure 6C and D, respectively, and clearly have

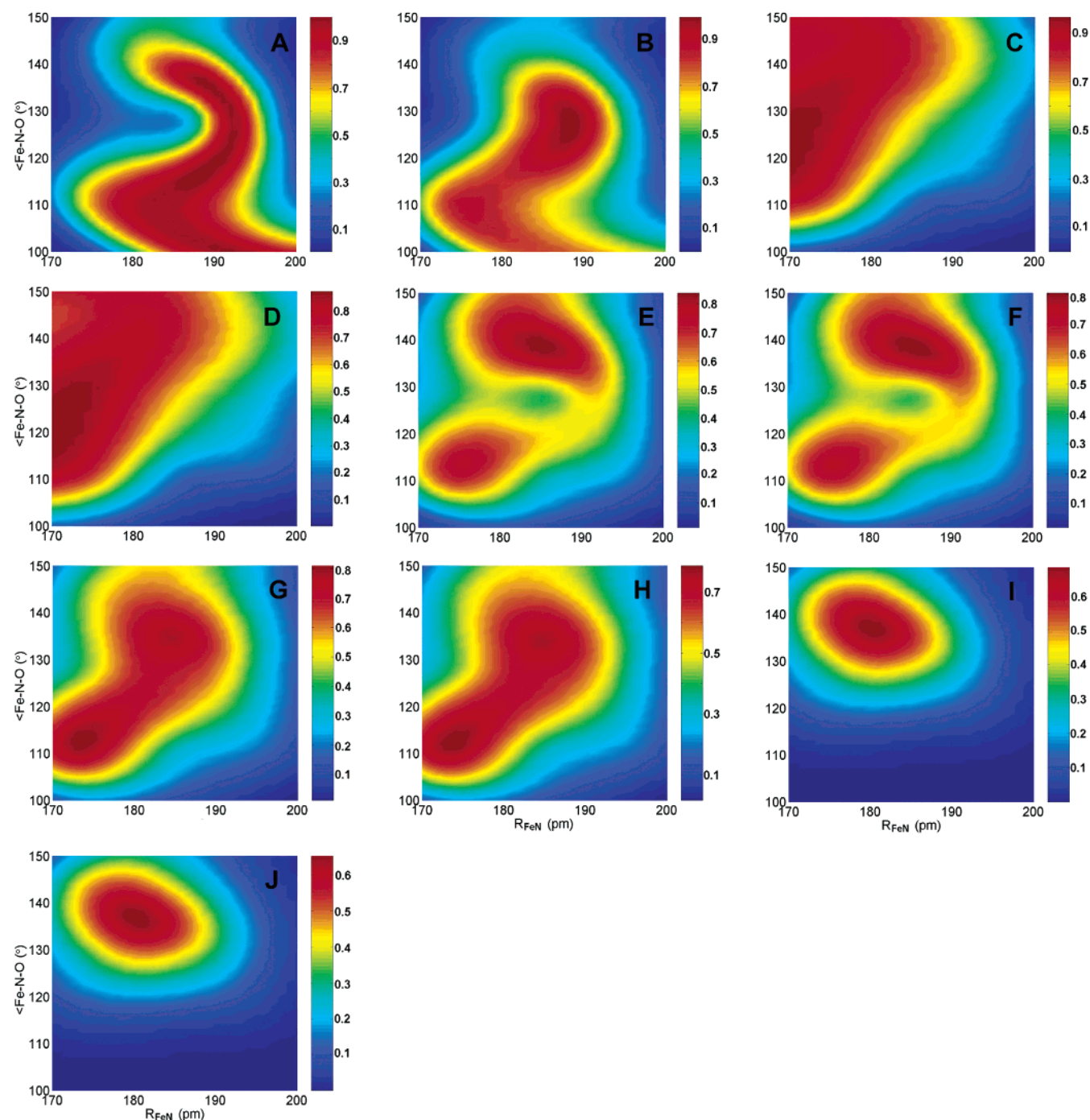


Figure 6. n Z-surface for HbNO: (A) 2 Z-surface of ΔE_Q and δ_{Fe} (4.2 K); (B) 2 Z-surface of ΔE_Q and δ_{Fe} (100 K); (C) 3 Z-surface of A_{11} , A_{22} , and A_{33} (α -subunit); (D) 3 Z-surface of A_{11} , A_{22} , and A_{33} (β -subunit); (E) 5 Z-surface of all five spectroscopic observables (α -subunit, 4.2 K); (F) 5 Z-surface of all five spectroscopic observables (β -subunit, 100 K); (G) 5 Z-surface of all five spectroscopic observables (α -subunit, 100 K); (H) 5 Z-surface of all five spectroscopic observables (β -subunit, 100 K); (I) 6 Z-surface of all five spectroscopic observables and the energy (α -subunit, 100 K); (J) 6 Z-surface of all five spectroscopic observables and the energy (β -subunit, 100 K). Colors reflect the probabilities, from eq 12.

maxima at ~ 1.72 Å, $\sim 130^\circ$. When both the Mössbauer and EPR results are combined, we obtain the 5 Z 4.2 K results shown in Figure 6E (α) and 6F(β), and at 100 K, the results of Figure 6G (α) and 6H (β) are obtained. These results are summarized in Table 3 where they can be compared with model and other protein results. Since the EPR results were obtained at 85 K, it seems likely that the 5 Z-surfaces shown in Figure 6G,H will be most accurate, since they combine 100 K Mössbauer with 85 K EPR experiments. Although here we have combined both human HbNO (EPR) and rat HbNO (Mössbauer) data here, it

seems quite unlikely that there will be species-dependent effects on the Mössbauer spectra, based on, for example, the observation that the Mössbauer spectra of (deoxy) hemoglobins from 10 different species are indistinguishable,⁴⁷ and all variable amino acids are very distant from the Fe site.

The results shown in Figure 6G,H indicate then, based solely on the Mössbauer and EPR data (the 5 Z-surfaces), that there are two mathematically probable solutions for r , β , as shown

(47) Kent, T.; Spartalian, K.; Lang, G.; Yonetani, T. *Biochim. Biophys. Acta* **1977**, *490*, 331–340.

Table 3. Structural Results for Six-Coordinate Model Compounds and Nitrosylheme Proteins

system	method ^a	R_{FeN} (Å)	$\angle\text{Fe-N-O}$ (deg)	reference
Fe(P)(1-MeIm)(NO)	⁵ Z-surface (α , 4.2 K)	1.85	139	this work
	⁵ Z-surface (β , 4.2 K)	1.86	138	this work
	⁵ Z-surface (α , 100 K)	1.84 (1.74)	135 (113)	this work
	⁵ Z-surface (β , 100 K)	1.84 (1.74)	133 (113)	this work
	⁶ Z-surface (α , 100 K)	1.79	137	this work
	⁶ Z-surface (β , 100 K)	1.79	136	this work
Fe(TPP)(1-MeIm)(NO)	X-ray	1.743	138.3	14
		1.743	142.1	14
MbNO	X-ray (1.70 Å)	1.889	111.6	11
MbNO	X-ray (1.90 Å)	1.859	127.2	11
leghemoglobin-NO	X-ray (1.80 Å)	1.965	144.9	12
MbNO ^b	B3LYP optimized	1.781	138.1	this work
MbNO ^b	BPW91 optimized	1.756	137.3	this work
Fe(P)(Im)(NO)	DFT optimized	1.72	138	40

^a For protein X-ray structures, their resolutions are indicated in parentheses. ^b The heme, NO, and proximal and distal His residues were excised from the PDB file 1HJT, and a partial geometry optimization of the N, O, and distal His H(N) atoms was carried out as described in the text.

in Table 3. One has an elongated Fe–NO bond length (1.84 Å) but a normal β Fe–N–O bond angle (135°) while the other has a normal Fe–NO bond length (1.74 Å) but a very bent β Fe–N–O (113°). However, the latter solution can be effectively removed by using the energy Z-surface, yielding the ⁶Z-surfaces shown in Figure 6I,J in which we find $r = 1.79$ Å for both α and β subunits and $\beta = 137^\circ$ (α) or $\beta = 136^\circ$ (β). These values are now clearly within the canonical range described previously for model systems⁷ and are quite close to the values found in the X-ray structure of Fe(TPP)(1-MeIm)(NO): $r = 1.74_3$ Å and $\beta = 138.3^\circ, 142.1^\circ$, with the more highly distorted ($\beta = 113^\circ$) protein structure being eliminated due to its high (~ 15 kcal mol⁻¹) energy penalty. On the other hand, a slight bond elongation is clearly permissible, based on the shape of the energy surface shown in Figure 4E, which allows for a modest bond elongation in this region of r, β space, due perhaps to the effects of hydrogen bonding to the distal histidine residue.

These values are, however, rather different to those determined crystallographically in a variety of other NO heme proteins, Table 3. While these values could all in principle be accurate, in some cases the bond angles are highly distorted (e.g. 111.6°, 127.2°) or the bond lengths are very long (e.g. 1.889 Å, 1.965 Å; Table 3) and these bond angle and bond length distortions will carry energy penalties in the ~ 5 –15 kcal mol⁻¹ range, too large to be accounted for simply by H-bonding.

To test in more detail to what extent H-bonding of NO to the distal His might actually change the Fe–NO bond length (and the NO bond length and Fe–N–O bond angle), we next carried out a geometry optimization study of one of these systems, a nitrosyl myoglobin (PDB file 1HJT).¹¹ This structure has a long Fe–NO bond length (1.889 Å) and an unusually bent Fe–N–O bond angle (111.6°). The heme, NO, and proximal and distal His residues were excised from the PDB file, and a partial geometry optimization of the N, O, and distal His H(N) atoms was carried out using the same large-scale basis described above and initially, with the B3LYP functional. The results for the geometry optimized structure are shown in Table 3 where they can be compared with a variety of other protein and six-coordinate model compound structure parameters. Of particular interest, we find that, upon geometry optimization, the Fe–NO bond length decreases from the crystallographic 1.889 Å to 1.781 Å and the Fe–N–O bond angle increases, from the crystallographic 111.6° to 138.1°. The bond angle determined in this way for MbNO is essentially identical to that

deduced by using the Z-surface approach on HbNO (with the energy filter). Likewise, the Fe–NO bond length (1.78 Å) is about the same as that we find for HbNO (1.79 Å), with both being longer than the bond lengths found in small molecule six-coordinate Fe(II) metalloporphyrins containing nitrogen-base ligands. The geometry optimized bond length is also slightly longer than that found previously for an Fe(P)(Im)(NO) structure optimized without the distal His.⁴⁰ Compared to this B3LYP optimized structure, using the pure density functional BPW91 for the geometry, optimization yielded an even shorter Fe–NO bond length, 1.756 Å, very similar to that found in the X-ray structure of the model compound, Fe(TPP)(1-MeIm)(NO),¹⁴ 1.743 Å (Table 3). The Fe–N–O bond angle (137.3°) in this case was also again very close to the value found in the six-coordinate model complex, Table 3.¹⁴ Taken together then, the results of the Z-surface predictions, together with the geometry optimization results, strongly suggest that both fully ligated nitrosylhemoglobin and nitrosylmyoglobin have Fe–N–O bond angles of ~ 136 – 138° and Fe–NO bond lengths in the 1.76–1.79 Å range, slightly longer than those observed in model systems which lack distal hydrogen bond donors.

Finally, we also investigated some of the molecular orbitals and spin densities in the nitrosylmetalloporphyrins studied here. Typical results for the α -HOMO, β -LUMO, and the total spin density for the $S = 1/2$ Fe(II)(NO)(imidazole) complex used in the H-bond geometry optimization study described above are shown in Figure 7A–C, respectively. These results are very similar to those we reported previously for the five-coordinate Fe(II)(OEP)(NO) based structure and indicate a major contribution of the d_{z^2} orbital to the HOMO.²⁷ However, in each of the six coordinate molecules, we also found, not surprisingly, a small contribution from the proximal imidazole ligand to the α -HOMO, basically as shown in Figure 7A. Moreover, the hydrogen-bonded distal imidazole was found to have a weak interaction with NO, again as shown in Figure 7A. In all cases, the spin densities were overwhelmingly located in the Fe and NO orbitals (see Figure 7C) and resemble the shape of the β -LUMO (Figure 7B), as noted previously for several other $S = 1/2$ systems.^{27,29}

Conclusions

The results we have obtained above are of interest for a number of reasons. First, we have carried out the first extensive density functional theory investigation of a broad variety of five-

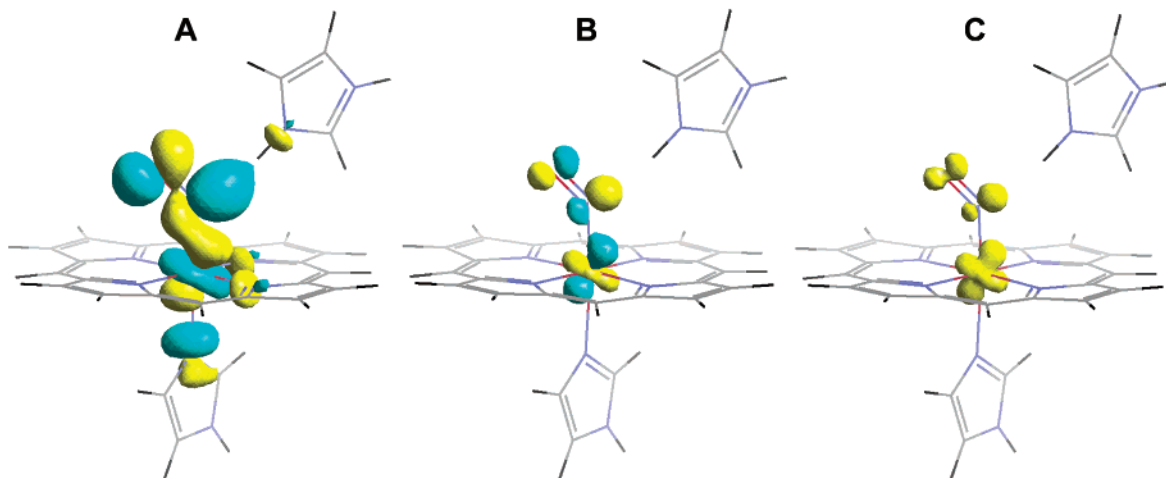


Figure 7. Spin density and MO isosurface representations for the hydrogen bonded $\text{Fe}(\text{P}(\text{Im})_2(\text{NO}))$ in MbNO (1HJT). (A) α -HOMO; (B) β -LUMO; (C) total spin densities (contour values = ± 0.04 , ± 0.1 , and $+0.02$ au, respectively).

and six-coordinate nitrosylmetalloporphyrins. In particular, we have used DFT methods to predict the Mössbauer quadrupole splittings, the Mössbauer isomer shifts, and, in one case, the EPR hyperfine coupling tensor components (A_{ii}), finding in most cases good agreement between theory and experiment. Second, the errors which were observed in the Mössbauer calculations were shown to correlate with uncertainties in the experimental crystallographic structures, as described by conventional crystallographic R_1 values. Third, we have calculated a series of property surfaces: how the quadrupole splittings, isomer shifts, and hyperfine coupling tensor components (A_{ii}) vary as a function of Fe–NO bond length and Fe–N–O bond angle in a model, six-coordinate $\text{Fe}(\text{II})(\text{NO})(\text{imidazole})$ complex. From these surfaces, we calculated Z-surfaces or probability surfaces which, together with knowledge of experimental Mössbauer and EPR spectroscopic properties (and energetic considerations) enabled determination of the most likely experimental geometries to be found in the proteins NO hemoglobin (fully ligated) and NO myoglobin. The results indicate that the Fe–N–O bond angle in nitrosylhemoglobin is about 136 – 137° while the Fe–NO bond length is about 1.79 Å (at 100 K). Fourth, we carried out a geometry optimization study of a nitrosylmyoglobin model, including the effects of hydrogen bonding from the distal His, and found essentially the same bond angle (137 – 138°) and bond length (1.76 – 1.78 Å) to that found in hemoglobin. The presence of the hydrogen bond interaction elongates the bond length by ~ 0.05 Å. Fifth, the results of the calculations imply a large energy penalty for very small Fe–N–O bond angles (~ 15 kcal mol^{-1} at $\beta = 111^\circ$). Sixth, we investigated the molecular orbitals

and spin densities in each system and found generally similar MO features for both five- and six-coordinate species. The unpaired spin density in the six-coordinate H-bonded model showed little spin density on either the proximal or distal imidazoles, with the spin density mapping the β -LUMO, while antibonding orbital interactions between both the proximal and distal imidazoles with the Fe–NO heme were seen in the α -HOMO. Overall, these results extend the Z-surface approach used previously to study Fe–CO bonding in diamagnetic heme proteins to paramagnetic Fe–NO proteins where, unlike the case of the diamagnetic systems, EPR hyperfine couplings can also be used as structure probes. The results obtained show a remarkable similarity in Fe–N–O bond angles between HbNO, MbNO, and simple model compounds, but with a somewhat lengthened Fe–NO bond distance, due most likely to an H-bond interaction with the distal His (or imidazole) residues. The ability to probe the details of Fe–N–O interactions in heme proteins should be of interest in the context of improving our understanding of the physiological effects of NO in the regulation of vascular tension, by providing atomic level probes of Fe–N–O structure and bonding in paramagnetic NO metalloproteins.

Acknowledgment. This work was supported in part by the United States Public Health Service (NIH Grant EB-00271-25).

Supporting Information Available: Expanded versions of Figures 4–6 with numbered contours. This material is available free of charge via the Internet at <http://pubs.acs.org>.

JA030340V